Available online at www.sciencedirect.com

ScienceDirect

Procedia Structural Integrity 47 (2023) 238–246

Structural Integrity Procedia

www.elsevier.com/locate/procedia

27th International Conference on Fracture and Structural Integrity (IGF27)

Experimental characterization and modelling of cyclic elastoplastic response of an AISI 316L steel lattice structure produced by laser-powder bed fusion

Marco Pelegatti[a]*, Denis Benasciutti[b], Francesco De Bona[a], Enrico Salvati[a]

[a]*Department Polytechnic of Engineering and Architecture, University of Udine, via delle Scienze 208, 33100 Udine, Italy*
[b]*Department of Engineering, University of Ferrara, via Saragat 1, 44122 Ferrara, Italy*

Abstract

In the last few years, many studies have been devoted to elucidating the mechanical properties of lattice structures produced by additive manufacturing (AM) techniques. Nevertheless, virtually none of the works dealt with the cyclic elastoplastic response, which is instead the focus of the present study. An AISI 316L steel FBCCZ (face and body-centered cell with vertical struts along the z-axis) lattice structure, produced by the AM technique laser-powder bed fusion (L-PBF), was experimentally tested and modelled using the finite element method. The mechanical behavior of the L-PBF AISI 316L steel was described by a non-linear kinematic (Chaboche's model) and isotropic (Voce's model) hardening model. Numerical results and their comparison with experimental evidence suggested that the study of a single unit cell by exploiting the periodicity condition can be severely impaired by the numerousness of the cells involved. More faithful models, accounting for the sample's edges effects, and including the effective dimension of the fabricated features by AM, lead to a highly satisfactory match, thus confirming the applicability of the proposed approach.

Keywords: laser-powder bed fusion; AISI 316L steel; cyclic plasticity; lattice structure; FE model

* Corresponding author.
E-mail address: pelegatti.marco@spes.uniud.it

10.1016/j.prostr.2023.07.101

1. Introduction

AM refers to all the manufacturing processes that build mechanical parts by adding material in a layer-by-layer fashion. Several techniques fit the definition of AM, and a wide range of materials can be processed (Gibson et al. (2015)). Amongst the AM techniques, the laser-powder bed fusion (L-PBF) of metallic materials has attracted the most attention. During the process, metals produced by AM experience a complex thermal history, which makes the fabricated materials exhibit different microstructures and mechanical properties than conventionally processed counterparts (Krakhmalev and Kazantseva (2021)). Therefore, a detailed mechanical characterization of materials produced by this technique is a mandatory requirement to ensure a truthful representation of their behavior. Such a qualification is not only needed when dealing with fully homogeneous AM materials, but also when the description of the mechanical properties of architected cellular materials is sought. Cellular materials are not material in a traditional way, but they build upon unit cells arranged in a regular pattern in space (Fleck et al. (2010)), also known as *metamaterials*. The manufacturing of this class of materials is taken to an unprecedented level of flexibility by exploiting the capabilities of AM processes, at different length-scales; the geometry of the unit cell can be highly complex, with features sizing from the (sub)micron scale up to the millimeter scale and above. Such materials can be tailored to improve the performance of engineering components in a wide range of applications (Du Plessis et al. (2022)). For instance, in biomedical sectors, lattice structures can be employed to reduce the stress-shielding effect and improve bone integration. They also seem promising in heat exchangers to enhance heat transfer. Other frequently reported applications highlight their remarkable efficiency when employed as impact absorbers and dampers to control vibrations. Overall, the main benefit of using lattice structures appears to be the lightweight of the component without losing performance in selected applications.

Although metamaterials appear highly non-homogenous at the unit cell scale, they can be treated as homogeneous materials at the component level as long as a length-scale separation between a single cell and the component exists, and the field variables are periodic at the cell scale. In that context, a large number of studies can be found in the recent literature dealing with the mechanical testing of lattice specimens, mostly limited to the analysis of quasi-static compression/tension properties though. Only in the last few years, the focus has been switching to the fatigue properties of these materials (Benedetti et al. (2021)), and now uniaxial high cycle fatigue tests on lattice specimens are commonly performed under compression-compression and tension-compression in load control. However, although during high cycle fatigue the material is globally subjected exclusively to elastic deformation, at the unit cell scale some regions may undergo plastic deformation due to the presence of small geometrical features. For this reason, the elastoplastic characterization of metamaterials is of great importance even in contexts that fall outside the low cycle fatigue (LCF) regime or other applications involving large plastic deformations, e.g., impact absorbers or components subjected to thermomechanical loads.

The cyclic elastoplastic response of cellular structures has been previously studied by Tomažinčič et al. (2019) and Tomažinčič et al. (2020), who carried out both experimental and numerical analyses. Nonetheless, the cellular structures in these works were obtained by cutting rolled plates of Al alloy with a water-jet machine. Furthermore, the tested specimens were characterized by a two-dimensional cellular structure since only a layer of cells was present in one of the three dimensions. To the best of the authors' knowledge, the experimental cyclic elastoplastic response of lattice structures fabricated by AM has not been investigated yet. In fact, amongst the few very recent articles focused on the subject, only numerical results are reported without any experimental validation (Molavitabrizi et al. (2022) and Zhang et al. (2022)).

This work provides a first attempt to experimentally and numerically characterize the cyclic elastoplastic response of a lattice structure obtained by L-PBF. One lattice-based cellular specimen was tested under cyclic tension-compression loading, in strain control mode, until the complete separation of the two clamped ends (LCF test). The material used to produce the lattice specimen is an AISI 316L stainless steel, whose material's intrinsic mechanical behavior (i.e., full-density) was previously unveiled by Pelegatti et al. (2022), including the calibration of the cyclic plasticity model (Pelegatti et al. (2023)). Such a materials model allowed for the finite element (FE) simulation of the cyclic elastoplastic response of the studied lattice structure. An extensive study on the suitability of periodic boundary conditions and other less simplified solutions, on the FE model, is covered to provide insight into aspects to consider when modelling these materials.

2. Material and methods

2.1. Material and lattice specimen

The geometry of the studied lattice specimen is reported in Fig. 1 (a) and consists of a lattice part of 4×4×15 cells and solid ends, entirely made of AISI 316L steel. Fig. 1 (b) displays the CAD geometry of the lattice cell, called FBCCZ (face and body-centered cell with vertical struts along the z-axis). The cell has a side length of 4 mm, and a nominal diameter of the struts of 1.1 mm, leading to a relative density of approximately 51%. The process parameters used to print the specimen can be found in Scalzo et al. (2021) – the same parameter used to produce the bulk material that had been previously characterized by Pelegatti et al. (2022) apart from the contouring which is only present in the lattice specimen. Likewise the full-density specimens, the lattice specimen underwent a stress-relief treatment at 550°C for 6 hours.

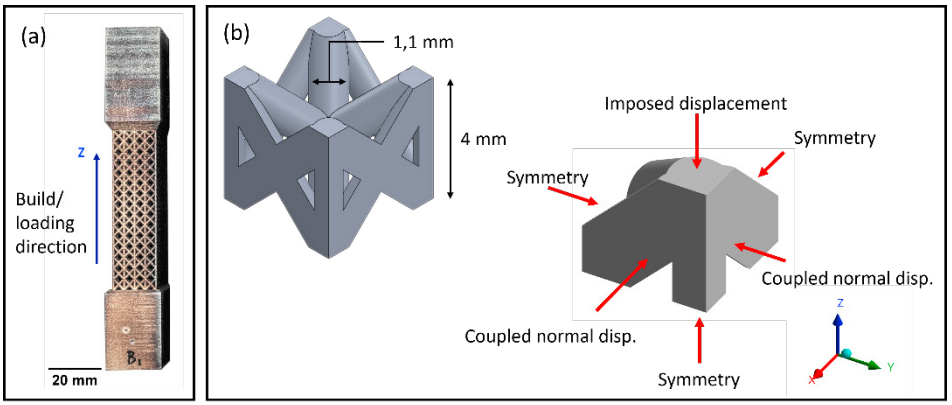

Fig. 1. (a) Geometry of the lattice specimen; (b) CAD geometry of the FBCCZ cell and an eight of the unit cell used in the FE model.

2.2. Experimental setup: LCF test

One lattice specimen was tested in LCF conditions under symmetric tension-compression in strain control mode. The strain amplitude imposed during the test was 0.7%, and the strain rate was equal to 4×10^{-3} s^{-1}. The experimental setup is depicted in Fig. 2 (a). The testing machine used for the LCF test is a servohydraulic MTS 810 System equipped with a 100 kN load cell. The axial strain was controlled using an MTS 634 model extensometer with a 25 mm gauge length. As previously stated, LCF tests at different strain amplitudes were also carried out on the full-density specimens. Interested readers can find more information about the experimental results in Pelegatti et al. (2022).

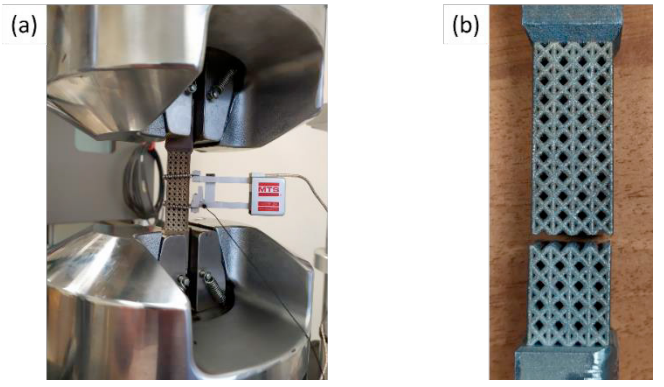

Fig. 2. (a) Experimental setup for the cyclic test; (b) Lattice specimen after final failure.

2.3. FE model: Unit cell and 4×4×1 structure

The cyclic elastoplastic response of the lattice structure was simulated using a FE model of a unit cell. The software used for the simulation was Ansys. Only an eighth of the cell was modelled, exploiting the symmetries of three planes (see Fig. 1 (b)). A mesh-independence study was carried out, considering the reaction force of the cell as the monitored variable. As a result, the chosen mesh consisted of 19256 10-node tetrahedral elements with an average size of 0.15 mm, totaling 28912 nodes. Coupling constraints were imposed on the nodes of the two remaining lateral faces for the displacement along the direction normal to the faces to mimic periodic boundary conditions. Finally, the load was imposed as a vertical cyclic displacement over the upper face.

Rate-independent elastoplastic simulations were performed using the theory of small displacements and small strains. The material was supposed to be isotropic linear elastic, and its yield behavior is assumed isotropic and represented by a Von Mises yield surface. The cyclic plastic response was simulated using non-linear kinematic and isotropic hardening models proposed by Chaboche et al. (1986) and Voce et al. (1948), respectively. For the sake of completeness, the incremental form of the two models is given:

$$d\boldsymbol{X} = \sum_{i=1}^{3} \frac{2}{3} C_i d\boldsymbol{\varepsilon_{pl}} - \gamma_i \boldsymbol{X_i} dp \tag{1}$$

$$dR = b(R_\infty - R)dp \tag{2}$$

where the second-order tensor $\boldsymbol{X}$, called back stress, is associated with kinematic hardening, whereas the scalar variable R with isotropic hardening. The change of the hardening variables is related to the increment of accumulated equivalent plastic strain, p, and (or) the plastic strain tensor, $\boldsymbol{\varepsilon_{pl}}$. The material parameters to be calibrated on the experimental data are C_i, γ_i, b and R_∞.

The stress-strain cycles and the cyclic stress response, recorded during the LCF tests, provided the experimental data for calibrating the cyclic plasticity models. The calibration procedure, which was previously developed by Pelegatti et al. (2021) for a wrought AISI 316L steel, was then used to obtain the parameters of the cyclic plasticity models for the L-PBF AISI 316L. The mechanical properties estimated from our previous LCF tests on the full-density specimens are listed in Table 1 (Pelegatti et al. (2023)).

In order to attempt modelling the actual specimen geometry with superior accuracy, additional FE models of 4×4×1 cellular structures, distinguished by different aspects, were considered. These structures represent a single layer of 4×4 cells in the lattice specimen considered in this work. After a mesh convergence test, the discretization of the domain was carried out by employing an average element size of 0.15 mm. The symmetries of the structures were exploited to reduce the number of degrees of freedom.

Table 1. Mechanical properties of the L-PBF AISI 316L steel.

Elastic region		Kinematic hardening						Isotropic hardening	
$E\ (MPa)$	$\sigma_{y,0}\ (MPa)$	$C_1\ (MPa)$	γ_1	$C_2\ (MPa)$	γ_2	$C_3\ (MPa)$	γ_3	$R_\infty\ (MPa)$	b
194323	380	320000	5500	97000	1000	25000	150	-140	0.6128

3. Results and discussion

3.1. Lattice structure: Experiment versus simulation of a single unit cell

The lattice specimen loaded at a strain amplitude of 0.7% failed after 30 cycles with complete separation (see Fig. 2 (b)). Some of the experimental stress-strain cycles are presented in Fig. 3 (a), together with the response of the full-density specimen tested in the same conditions, whereas Fig. 3 (b) displays the simulated response for both the unit cell and bulk material. Concerning the lattice structure, the force was divided by the area of the lattice specimen (i.e. 16×16 mm^2) to obtain the stress (also called "macroscopic stress" in this work), whereas the strain was directly measured by the extensometer.

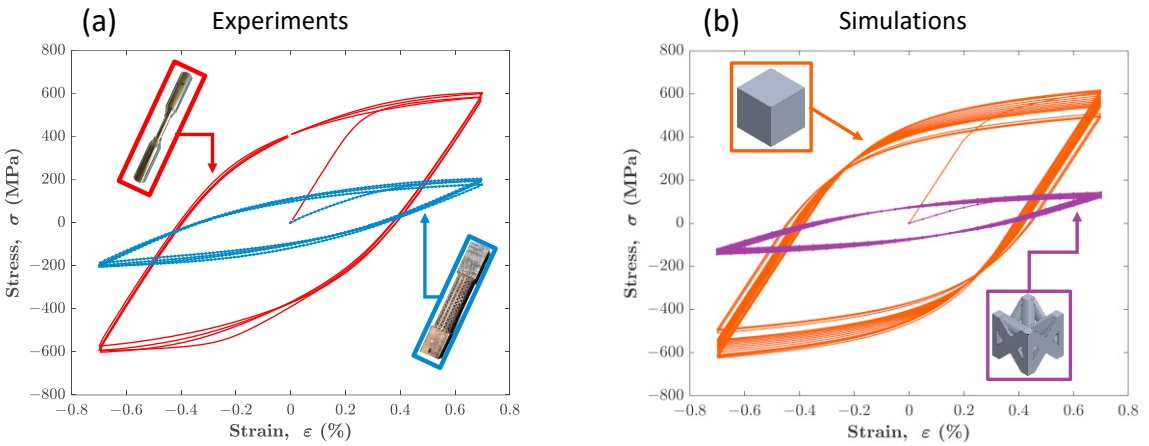

Fig. 3. (a) Experimental stress-strain cycles (1st, 5th, 10th, 20th) for the lattice and full-density specimen tested at 0.7% of strain amplitude; (b) Simulated stress-strain cycles (from 1st to 700th) for the lattice unit cell and bulk material imposing a 0.7% of strain amplitude.

A close comparison between the behavior of the lattice specimen and the simulated response using a unit cell is shown in Fig. 4, denoted by the numbers 1 and 2. Only the first quarter of the cycle of the cyclic test is presented, and it highlights a significant discrepancy between experimental and predicted stress-strain response. The relative error on the elastic modulus is as high as 31.5%, and it reduces to 26.7% on the stress value at 0.7% of strain. The relatively poor capability of the unit cell to capture the experimental response is explained by the low number of cells in the cross-section of the lattice specimen and the difference between the as-built and as-designed geometries. These two aspects will be discussed in the following Sections. However, it is worth noticing that despite the high degree of approximation of the FE model of the unit cell, this model maintains a low computational cost and seems the only possible choice if the cyclic behavior up to stabilization has to be investigated, especially for real applications involving a considerable number of unit cells. In any case, the simulation of the single unit cell showed that it is possible to adequately capture the shape of the stress-strain response, regardless of the relative error on the macroscopic stress.

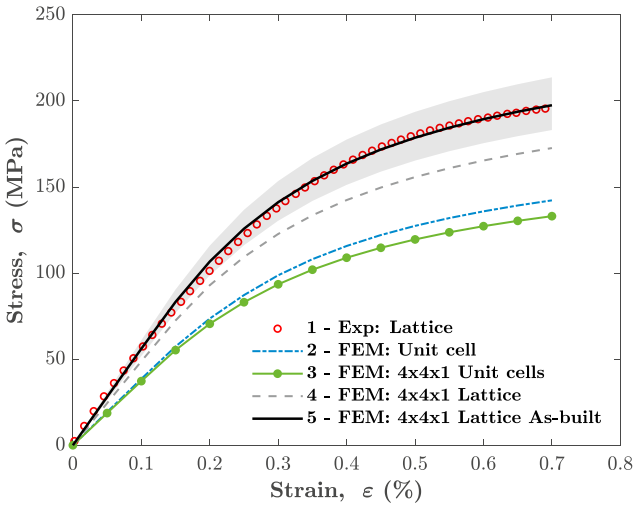

Fig. 4. Comparison between experimental and simulated monotonic stress-strain response with different FE models.

3.2. Number of cells & boundary effects

An improvement of the simulated response of the lattice structure can be achieved by modelling the entire cross-section of the lattice specimen. The two strategies that can be addressed for the lattice specimen considered in this study are now discussed. In both cases, the geometry of the FE model consists of a structure with 4×4×1 cells using symmetries. In the first strategy, the geometry is obtained by repeating the unit cell in the transversal plane and is referred to as "3 - FEM: 4×4×1 Unit cells" in Fig. 4. Meanwhile, the second possibility considers that the struts at the edges of the 4×4×1 structure are not truncated, therefore showing a fully circular cross-section. This geometry is closer to reality than the geometry obtained by repeating the unit cell and is labelled "4 - FEM: 4×4×1 Lattice" in Fig. 4.

Fig. 4 shows that the simulated response of the "4×4×1 Unit cells" structure gives a lower macroscopic stress as opposed to the unit cell with periodic boundary conditions. This result is due to the fact that the cells at the boundaries are free to deform in the direction orthogonal to the load and hence are less stiff than the unit cell. Therefore, the simulated response goes further away from the experimental data (see case number 3 in Fig. 4). On the other hand, the "4×4×1 Lattice" structure is closer to reality than the geometry obtained by repeating the unit cell. That difference in the geometry leads to a not negligible deviation between the macroscopic response of the unit cell and the 4×4 cross-section with complete struts at the boundaries. In fact, the complete struts at the boundaries considerably increase the stiffness of the FE model, and the simulation approaches the experimental behavior. Nevertheless, Fig. 4 displays that a relative error as high as 11% still exists on the macroscopic stress (see case number 4 in Fig. 4).

The abovementioned aspects are related to boundary effects and reveal that the simulated response using a single unit cell becomes sufficiently representative only if the number of cells in the lattice specimen is high enough. As mentioned before, the behavior of the cells at the boundaries is different compared to the unit cell with periodic boundary conditions and becomes negligible when the number of cells in the section increases. This statement was proved by simulating the response of lattice structures with an increasing number of cells in the section for the two approaches.

For the sake of showing the influence of the number of repeating unit cells on the macroscopic response, an additional simulation is performed, i.e., the 7×7×1 model. Fig. 5 (a) shows that the simulated macroscopic response of the "7×7×1 - Unit cells" structure is closer to the one of the unit cell if compared to the "4×4×1 - Unit cells". The same conclusion draws if the complete circular cross-section is considered for the struts at the boundaries, as reported again in Fig. 5 (a). The relative error between the stress response of the lattice structures and the unit cell is displayed in Fig. 5 (b). Considering the "n×n×1 – Lattice" structures, the influence is slower to disappear, and the relative error between the lattice structure and the unit cell remains more than 10% for 7×7×1 cells. On the other hand, the "7×7×1 - Unit cells" structure gives a maximum relative error lower than 4%.

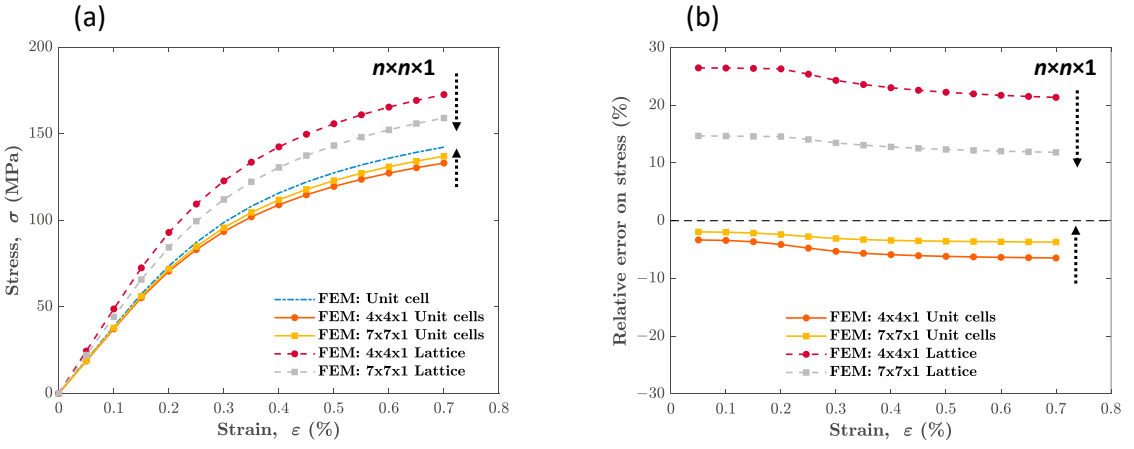

Fig. 5. (a) Comparison between the simulated stress-strain response using a unit cell and $n \times n \times 1$ lattice structures with increasing number of cells; (b) Relative error on macroscopic stress value between the $n \times n \times 1$ lattice structures and unit cell.

3.3. Dimensional and geometrical errors

The discussed modelling strategies point out two effects related to the cells at the boundaries, which tend to disappear when the number of cells in the section increases. Therefore, the simulated response using a single unit cell can be considered accurate only if the number of cells is high enough. However, a deviation between case number 4 and the experimental data still exists (see Fig. 4). This deviation can be explained by the dimensional and geometrical errors introduced by the manufacturing process between the "real" geometry of the as-built structure with the "ideal" one of the as-designed models. The best agreement between the experiment and simulation can be obtained if these dimensional errors are included in the FE model, which is case number 5 in Fig. 4. In summary, the same modelling approach of case number 4 is adopted, but the inclined struts of all the cells are modelled introducing a geometrical correction according to measurements of the as-built structures, which will be described in the following.

The dimensional and geometrical errors were observed and evaluated in the as-built lattice geometry. The results of this analysis are exhaustively reported in the work of Scalzo et al. (2021). It was noted that the cross-section of the tilted struts had almost an elliptical shape with a size in one of the axes (for simplicity, called "vertical" size) higher than the nominal diameter. The measured difference between the as-built and as-designed "vertical" sizes of the inclined struts is presented in Table 2 for the three analyzed lattice specimens. As a result of this mismatch, the greater the as-built "vertical" size of the inclined struts, the higher the axial and bending stiffness.

At this point, a rational correction was made to the geometry simulated by the FE method. Specifically, the circular section was maintained using an "equivalent" diameter. It is worth noting that the "equivalent" diameter cannot guarantee the same area and second moment of area of the elliptical section. Therefore, the "equivalent" diameter was calculated by imposing that the percentage difference between the area of the "equivalent" and elliptical section was equal to the percentage difference between the second moment of area of the "equivalent" and elliptical section. This approach resulted in an overestimated area of the "equivalent" section compared to the elliptical one, whereas the second moment of area is underestimated.

Finally, the inclined struts were increased by 0.0758 mm based on the mean value reported in Table 2, thus 1.1758 mm. Along with the results of this analysis, shown in Fig. 4 with the black line, a scatter band was evaluated (see the transparent band in the figure) by increasing the diameter by 0.1225 mm and 0.0326 mm, which correspond to the "equivalent" diameter considering the standard deviation of the dimensional error summed, and subtracted, to the mean value.

Table 2. Error between the as-designed and as-built "vertical" sizes of the inclined struts for three lattice specimens.

Replicate	Deviation on "vertical" size of inclined struts (mm)
1	0.042
2	0.138
3	0.189
Mean	0.123
Standard deviation	0.075

Considering that adjustment, the cyclic response of the lattice structure was also simulated and compared to the experimental data. This comparison is illustrated in Fig. 6 for the cyclic stress response and some stress-strain cycles, which are well represented by the simulation. Minimal discrepancies become evident only in the last cycles due to the onset of the fracture. For example, Fig. 6 displays the 20^{th} experimental cycle, which exhibited an asymmetry between the tensile-going and compressive-going phases. Specifically, the maximum stress in the cycle is lower than the minimum stress in absolute values. Furthermore, an inflection point in the compressive-going branch of the cycle is visible. As a final remark, it is worth mentioning that the simulation using a 4×4×1 structure is more computationally expensive than simulating a unit cell. As a matter of fact, a cyclic simulation of 30 cycles took more than 25 hours on a typical personal computer. Considering the same computational time, a cyclic simulation of a single unit cell can cover 700 cycles.

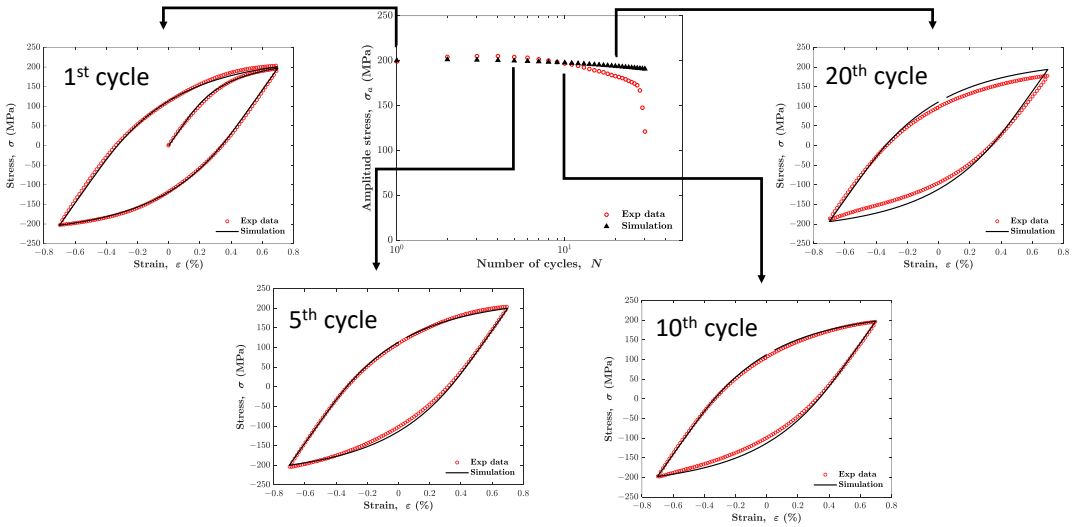

Fig. 6. Simulated cyclic response using a 4×4×1 structure including the dimensional errors versus the experimental behavior.

4. Conclusion

A lattice specimen with an FBCCZ cell topology made of AISI 316L steel was tested under cyclic tension-compression loading in strain control mode. The experimental results consist of stress-strain cycles of the lattice structure. Numerical models with different degrees of approximation were then developed to describe the experimental behavior. Chaboche and Voce's models were adopted to represent the cyclic elastoplastic behavior of the bulk material.

The simulated response using the FE model of a single unit cell with periodic boundary conditions gave significant discrepancies from the experimental data. Nonetheless, the shape of the stress-strain curve predicted by the FE model of a unit cell is accurate, and the stress values are almost purely scaled. This deviation can be related to the relatively low number of cells in the section of the experimentally tested lattice specimen and the difference between the as-built and as-designed lattice structure. In fact, the FE model of a structure with 4×4×1 cells, including the dimensional inaccuracies introduced by the manufacturing process, predicts the experimental cyclic response with high accuracy.

This study is the first of its kind and provided some important insights on the applicability of FE numerical simulations to accurately predict the cyclic elastoplastic behavior of additively manufactured metamaterials.

Acknowledgements

The authors would like to thank Federico Scalzo, Emanuele Vaglio, Giovanni Totis and Prof. Marco Sortino of the LAMA FVG laboratory of the University of Udine for providing the lattice specimen tested in this work. Additional thanks are due to Francesco Sordetti and Alex Lanzutti for helping with the mechanical test.

References

Benedetti, M., Du Plessis, A., Ritchie, R. O., Dallago, M., Razavi, S. M. J., Berto, F. 2021. Architected cellular materials: A review on their mechanical properties towards fatigue-tolerant design and fabrication. Materials Science and Engineering: R: Reports 144, 100606.

Chaboche, J. L. 1986. Time-independent constitutive theories for cyclic plasticity. International Journal of Plasticity 2, 149-188.

Du Plessis, A., Razavi, S. M. J., Benedetti, M., Murchio, S., Leary, M., Watson, M., Bathe, D., Berto, F. 2021. Properties and applications of additively manufactured metallic cellular materials: A review. Progress in Materials Science 125, 100918.

Fleck, N. A., Deshpande, V. S., Ashby, M. F. 2010. Micro-architectured materials: past, present and future. Proceedings of the Royal Society A: Mathematical, Physical and Engineering Sciences 466, 2495-2516.

Gibson, I., Rosen, D., Stucker, B., Khorasani, M., Rosen, D., Stucker, B., Khorasani, M. 2015. In: "*Additive manufacturing technologies*". Springer Cham.

Krakhmalev, P., Kazantseva, N. 2021. Microstructure of L-PBF alloys, in "*Fundamentals of laser powder bed fusion of metals"*. In: Yadroitsev, I., Yadroitsava, I., Du Plessis, A., MacDonald, E. (Eds.). Elsevier, pp. 215.

Molavitabrizi, D., Ekberg, A., Mousavi, S. M. 2022. Computational model for low cycle fatigue analysis of lattice materials: Incorporating theory of critical distance with elastoplastic homogenization. European Journal of Mechanics-A/Solids 92, 104480.

Pelegatti, M., Lanzutti, A., Salvati, E., Srnec Novak, J., De Bona, F., Benasciutti, D. 2021. Cyclic plasticity and low cycle fatigue of an AISI 316L stainless steel: Experimental evaluation of material parameters for durability design. Materials 14, 3588.

Pelegatti, M., Benasciutti, D., De Bona, F., Lanzutti, A., Magnan, M., Novak, J. S., Salvati, E., Sordetti, F., Sortino, M., Totis, G., Vaglio, E. 2022. On the factors influencing the elastoplastic cyclic response and low cycle fatigue failure of AISI 316L steel produced by laser-powder bed fusion. International Journal of Fatigue 165, 107224.

Pelegatti M, Benasciutti D, De Bona F, Lanzutti A, Novak JS, Salvati E. Strain-controlled fatigue loading of an additively manufactured AISI 316L steel: Cyclic plasticity model and strain–life curve with a comparison to the wrought material. *Fatigue Fract Eng Mater Struct*. 2023. https://doi.org/10.1111/ffe.13992

Scalzo, F., Totis, G., Vaglio, E., Sortino, M. 2021. Experimental study on the high-damping properties of metallic lattice structures obtained from SLM. Precision Engineering 71, 63-77.

Tomažinčič, D., Nečemer, B., Vesenjak, M., Klemenc, J. 2019. Low-cycle fatigue life of thin-plate auxetic cellular structures made from aluminium alloy 7075-T651. Fatigue & Fracture of Engineering Materials & Structures 42, 1022-1036.

Tomažinčič, D., Vesenjak, M., Klemenc, J. 2020. Prediction of static and low-cycle durability of porous cellular structures with positive and negative Poisson's ratios. Theoretical and Applied Fracture Mechanics 106, 102479.

Voce, E. 1948. The relationship between stress and strain for homogeneous deformation. Journal of the Institute of Metals 74, 537-562.

Zhang, P., Zhang, D. Z., Zhong, B. 2022. Constitutive and damage modelling of selective laser melted Ti-6Al-4V lattice structure subjected to low cycle fatigue. International Journal of Fatigue 159, 106800.